

Journal of Materials Chemistry C

Accepted Manuscript



This is an *Accepted Manuscript*, which has been through the Royal Society of Chemistry peer review process and has been accepted for publication.

Accepted Manuscripts are published online shortly after acceptance, before technical editing, formatting and proof reading. Using this free service, authors can make their results available to the community, in citable form, before we publish the edited article. We will replace this *Accepted Manuscript* with the edited and formatted *Advance Article* as soon as it is available.

You can find more information about *Accepted Manuscripts* in the [Information for Authors](#).

Please note that technical editing may introduce minor changes to the text and/or graphics, which may alter content. The journal's standard [Terms & Conditions](#) and the [Ethical guidelines](#) still apply. In no event shall the Royal Society of Chemistry be held responsible for any errors or omissions in this *Accepted Manuscript* or any consequences arising from the use of any information it contains.

Enhanced Optical Limiting and Carrier Dynamics in Metal Oxide-Hydrogen Exfoliated Graphene Hybrids

Benoy Anand,^a Adarsh Kaniyoor,^b Debasis Swain,^c Tessy Theres Baby,^b S. Venugopal Rao,^c
S. Siva Sankara Sai,^a Sundara Ramaprabhu,^b Reji Philip^{*d}

^a*Department of Physics, Sri Sathya Sai Institute of Higher Learning (SSSIHL), Prashanti Nilayam, Andhra Pradesh 515134, India*

^b*Alternative Energy and Nanotechnology Laboratory (AENL), Nano Functional Materials Technology Centre (NFMTC), Department of Physics, Indian Institute of Technology Madras (IITM), Chennai 600036, India*

^c*Advanced Center for Research in High Energy Materials (ACRHEM), University of Hyderabad, Hyderabad 500046, Andhra Pradesh, India*

^d*Light and Matter Physics Group, Raman Research Institute, C.V. Raman Avenue, Sadashivanagar, Bangalore 560080, India.*

ABSTRACT

Hydrogen exfoliated graphene (HEG) is an interesting class of few layer graphene which is synthesized *via* hydrogen induced simultaneous exfoliation-reduction of graphite oxide. HEG exhibits strong optical limiting (OL) due to defect states arising from the large number of structural defects as well as oxygen functionalities present on its surface. Recently we have shown that OL in HEG can be improved by simple acid functionalization, as it results in an increased number of defects. In the present study we demonstrate that the OL performance of functionalized HEG (*f*-HEG) can be further improved, in both short-pulse (nanosecond) and ultrafast (femtosecond) laser excitation regimes, by using hybrids of *f*-HEG with transition metal oxide nanoparticles (NPs) such as CuO. The enhancement in OL efficiency of the hybrid arises from strong nonlinear absorption in CuO NPs, which is determined mostly by interband and intraband transitions. The presence of defect states in the samples is confirmed using ultrafast pump-probe measurements which reveal a delayed carrier relaxation due to carrier trapping by these states. Furthermore, we also show that the occurrence of induced thermal scattering is

minimal in these water dispersed systems, so that OL occurs predominantly due to nonlinear absorption.

1. INTRODUCTION

It is now well established that reduction/exfoliation of graphite oxide by certain methods can result in the production of few layer graphene (FLG) like structures which are defective by nature.¹ Hydrogen exfoliated graphene (HEG) is an interesting class of such FLGs which is synthesized by hydrogen induced simultaneous exfoliation-reduction of graphite oxide.¹ Scalability of synthesis and large surface area ($\sim 442.9 \text{ m}^2/\text{g}$), together with excellent physical, chemical, and electronic properties, make HEG a potential candidate for a number of applications such as field emitters, nanofluids, and gas sensors.^{2,3} Its surface is generally wrinkled and defective due to harsh oxidation and exfoliation during the synthesis, which results in a prominent D band in the Raman spectrum.¹ In addition, there are functional groups ($\sim 6\text{-}8 \text{ wt. \%}$) like epoxy and -OH groups attached above and below the basal planes, and -COOH groups bound to the edges of the basal planes.¹ Presence of these remnant oxygen functionalities and the large number of structural defects lead to the display of unique nonlinear optical (NLO) properties by HEG, compared to graphene grown by other conventional methods. For example, HEG exhibits strong optical limiting (OL) behavior when excited by laser pulses of nanoseconds (ns) or femtoseconds (fs) duration,⁴ which is quite contrary to the saturable absorption (SA) behavior seen in epitaxially grown⁵ or chemical vapor deposited⁶ graphene. OL in HEG arises primarily due to strong nonlinear absorption (NLA), which is greatly influenced by the defects. Consequently, by increasing the number of defects through acid functionalization, OL performance of HEG can be enhanced.⁴

In an attempt to further improve the OL performance of functionalized HEG (*f*-HEG), metal decoration with Pt, Pd and Ag nanoparticles (NPs) has been tried recently.^{4,7} Pt and Pd NPs enhance OL in *f*-HEG by strong interband transitions between the *d* band and *s-p* band, and charge transfer across the metal-HEG interface.⁴ Picosecond Z-scan measurements carried out in HEG-Ag NP composites revealed that NLA can be manipulated by selectively coupling the incident wavelength to the localized surface plasmon modes of the NPs.⁷ The key idea is to enhance the overall NLA in the hybrid system, which in turn improves its OL performance. In

this regard transition metal oxide (TMO) NPs are promising as they are thermally and chemically stable, and possess excellent nonlinear optical properties.⁸ Therefore, it is highly desirable to make water dispersible hybrids of *f*-HEG with TMO NPs for developing practical ‘solution processable’ optical limiters with superior limiting performance. It is expected that the electronic, thermal and optical properties can be tuned by interfacing HEG with electron-rich TMO NPs. Additionally, these NPs prevent the restacking of individual HEG sheets and increase the surface area, thereby improving the performance of the hybrids in practical applications. In fact it was recently shown that ZnO decoration enhances OL in the case of reduced graphene oxide.⁹

Among the various TMOs, CuO NPs are of particular interest due to their excellent electronic,¹⁰ electrochemical¹¹ and third order nonlinear optical⁸ properties, which have received tremendous technological attention. The physiochemical properties of CuO such as the photoconductivity and the photochemistry can be tailored for fabricating optical switches and solar cells. Composites of CuO NPs with *f*-HEG have previously been studied by Baby *et al.* for field emission and transport properties.^{2,3} The thermal conductivity of *f*-HEG is improved significantly with metal oxide decoration, making these composites suitable for coolant applications.³ It is observed that decoration with CuO reduces the work function of *f*-HEG composite and increases its surface roughness, thus enhancing field emission.² In the present paper, we report the third order NLO properties of *f*-HEG-CuO NP hybrid (CuO/*f*-HEG) dispersed in water. We demonstrate that decoration with CuO NPs enhances NLA in *f*-HEG, yielding more efficient optical limiters. Moreover, we attempt to correlate various important factors such as defects in HEG, absorption characteristics of CuO NPs, interaction between *f*-HEG and NPs, and electron dynamics in the hybrid, to the observed enhancement in OL.

2. EXPERIMENTAL METHODS

2.1. Material synthesis

HEG is synthesized by hydrogen induced simultaneous exfoliation-reduction of graphite oxide as explained elsewhere.¹ As-synthesized HEG is treated with concentrated sulphuric acid and nitric acid (3:1 by vol.) to obtain *f*-HEG. CuO/*f*-HEG hybrid is synthesized as follows. 200 mg of copper chloride is added to 20 ml of de-ionized (DI) water and sonicated for 5 min. The dispersion is then added to 200 mg of *f*-HEG dispersed in 20 ml of DI water, which is again

sonicated for 30 min. The colloidal solution is then stirred for 24 h during which copper is reduced from CuCl_3 by using a reducing solution, which is a mixture of 1M NaBH_4 and 0.1M NaOH . Once the reduction reaction is over, the colloidal solution is washed with DI water and filtered using cellulose membrane filter. The material obtained is further dried at 70 °C under vacuum for 6 h. The final product is annealed at 350 °C for 2 h.

2.2. Characterization techniques

Powder X-ray diffraction studies are carried out using X'Pert PRO, PANalytical diffractometer with nickel-filtered $\text{Cu K}\alpha$ radiation as the X-ray source. The sample is scanned in steps of 0.016° in the 2θ range of 10 to 90 degrees. Raman spectra are obtained with a WITEC alpha 300 Confocal Raman system equipped with an Nd:YAG laser (532 nm) as the excitation source. Transmission electron microscopy studies are carried out using a TECNAI F-20 (S-TWIN) instrument. For TEM measurement, the powder samples are dispersed in absolute ethanol using mild ultrasonication and casted onto carbon coated Cu grid (SPI supplies, 200 mesh).

2.3. NLO measurements

The open aperture Z-scan technique is employed to study the NLO characteristics of the *f*-HEG-metal oxide hybrid. Excitation is by linearly polarized laser pulses of 5 ns duration at 532 nm, and 100 fs duration at 800 nm, respectively. Successive laser pulses excite the samples at a repetition rate of less than 0.5 Hz. From repeated knife edge measurements, the beam waist at focus was calculated to be $\sim 20 \mu\text{m}$ for the ns pulses and $\sim 16 \mu\text{m}$ for the fs pulses. For nonlinear transmission measurements, samples which are uniformly dispersed in water are taken in 1 mm thick quartz cuvettes. Appropriate concentrations are used such that the linear transmittance of the dispersions is the same (70%) at both excitation wavelengths. A detailed description of our Z-scan set up can be found in Ref. 12.

2.4. Ultrafast pump-probe measurements

The experimental setup used for time resolved differential transmission measurements is detailed elsewhere.¹³ Briefly, ultrafast laser pulses of ~ 70 fs duration at 580 nm are used for pumping as well as probing. These are derived from an optical parametric amplifier (TOPAS-C, Light Conversion) working at a repetition rate of 1 kHz, which is pumped by a Ti:sapphire regenerative amplifier. For maximum overlap the pump and probe diameters are kept at ~ 3 mm

and ~ 1 mm, respectively, and the angle between them is reduced to $\sim 3^\circ$. The energy ratio of pump and probe beams is maintained at 10:1 with the probe power being 0.5 mW. The pump and probe beams are focused onto the sample solution kept in a 5 mm thick cuvette using converging lenses of 20 cm and 15 cm focal lengths, respectively. The pump beam is modulated at 109 Hz using a mechanical chopper. Intensity of the transmitted probe is measured as a function of time delay between the pump and probe pulses using a Si-PIN diode with lock-in detection. Polarizations of the pump and probe beams are kept perpendicular to each other to prevent scattered pump light from reaching the detector.

3. RESULTS AND DISCUSSION

3.1. Material characterization

Powder X-ray diffraction patterns of *f*-HEG and CuO/*f*-HEG are shown in Figure 1a. *f*-HEG has its characteristic (002) peak centered at 25° . Shift from the traditional sharp and intense graphitic peak at 26.5° suggests the absence of severe stacking along the *c*-axis, and a reduction in the crystallite size. Graphite typically contains about 100 to 200 layers along the *c*-axis whereas after exfoliation the sample contains only 5 to 10 layers. Moreover, while the graphite used has a flake size of 45 μm , HEG obtained has a flake size of only about 1-2 μm . Additional peaks, corresponding to CuO, can be seen at $2\theta > 25^\circ$ after decoration with copper oxide which suggest the intense crystallinity of NPs. The crystal structure of CuO is monoclinic, and the crystallite size calculated using the Scherrer equation is ~ 18 nm.

Figure 1b shows the measured Raman spectra of CuO/*f*-HEG and *f*-HEG (the Raman spectrum of *f*-HEG is described elsewhere).^{2,3} In brief, *f*-HEG exhibits a Raman spectrum similar to that of graphite oxide with broad D and G bands and a flat 2D region. This is indicative of the presence of large amount of defects as well as functional groups which disturb the hexagonal network of graphene. As a result, the actual sp^2 carbon domain size is small, leading to the suppression of the 2D band. Upon metal oxide loading, small shifts and broadening are observed in the D and G bands.³ This shift in CuO/*f*-HEG arises from the interaction of metal oxide nanoparticles with *f*-HEG sheets. It can also be seen that the peak intensity ratio of D and G bands (I_D/I_G) decreases from 1.12 ± 0.03 (*f*-HEG) to 0.95 ± 0.02 (CuO/*f*-HEG). Such reduction, which has been observed in other metal oxide - nanocarbon composites as well, is attributed to the reduction in the number of dangling bonds or other defect sites due to the attachment of

metal oxide nanoparticles.¹⁴ Figure 1c is the TEM image of CuO/*f*-HEG hybrid which clearly shows the uniform decoration of the HEG sheet by CuO nanoparticles. The metal oxide loading is maintained at 20 wt% which is confirmed by weighing the samples before and after the loading.

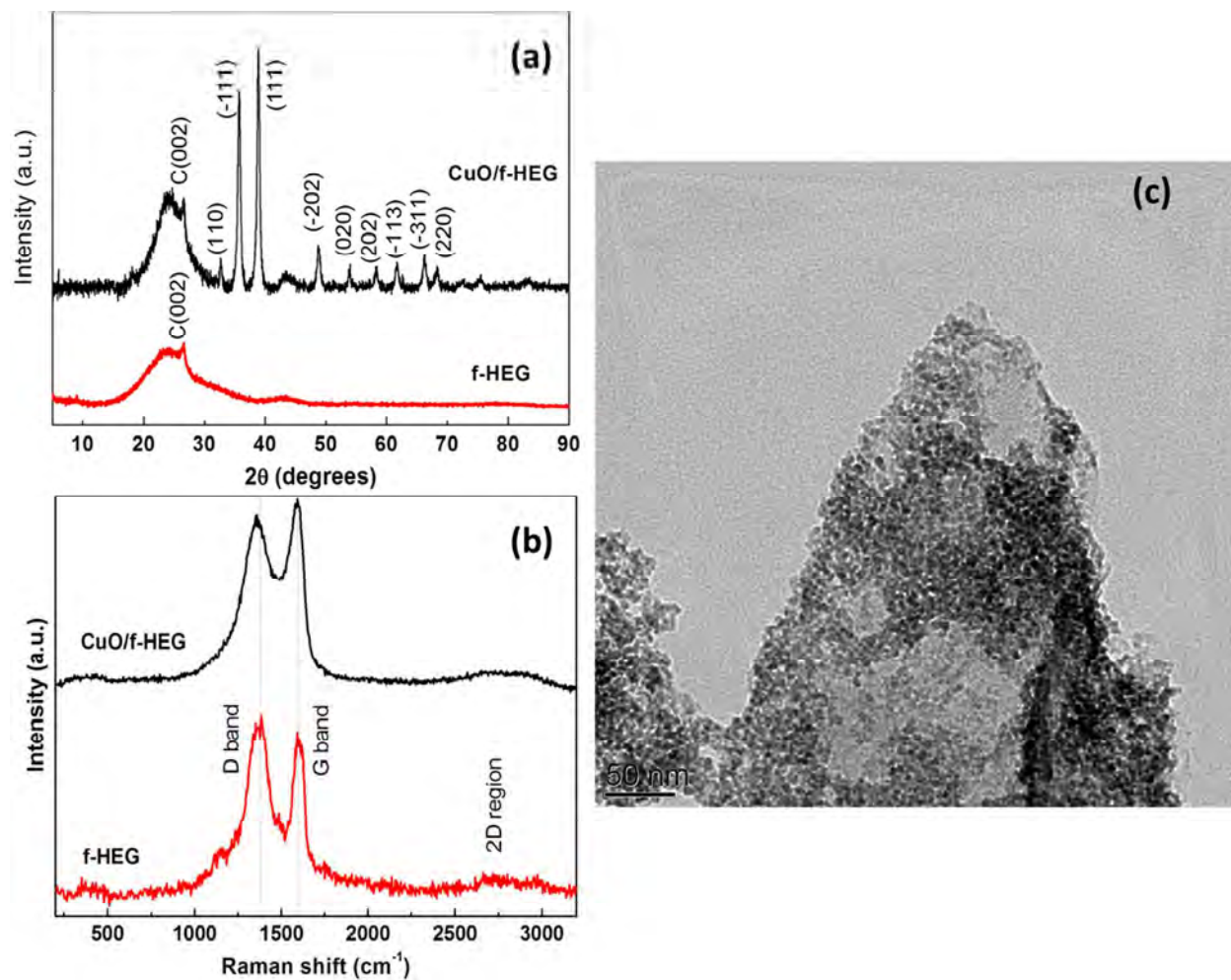


Figure 1. (a) XRD and (b) Raman spectra of *f*-HEG and CuO/*f*-HEG. (c) TEM image of CuO/*f*-HEG, showing uniform decoration of CuO nanoparticles on the HEG basal sheet.

3.2. Optical limiting in CuO/*f*-HEG hybrids

CuO/*f*-HEG exhibited excellent optical nonlinearity when excited by ‘ns’ as well as ‘fs’ laser pulses. The open aperture Z-scan curves of the samples plotted between sample position and normalized transmittance, in both ns and fs excitation regimes, are shown in Figures 2a and 2b, respectively. It is evident that light transmission decreases with increase in input light intensity

(which is highest at the beam focus, $z = 0$, and decreases uniformly in either direction), indicating a nonlinear response in both the excitation regimes. The semi-transparent nature of CuO/*f*-HEGs (linear transmittance of 70%) and the nonlinear transmission characteristics shown in Figures 2a and 2b suggest that CuO/*f*-HEG is an efficient optical limiter for short-pulse as well as ultrafast laser pulses.

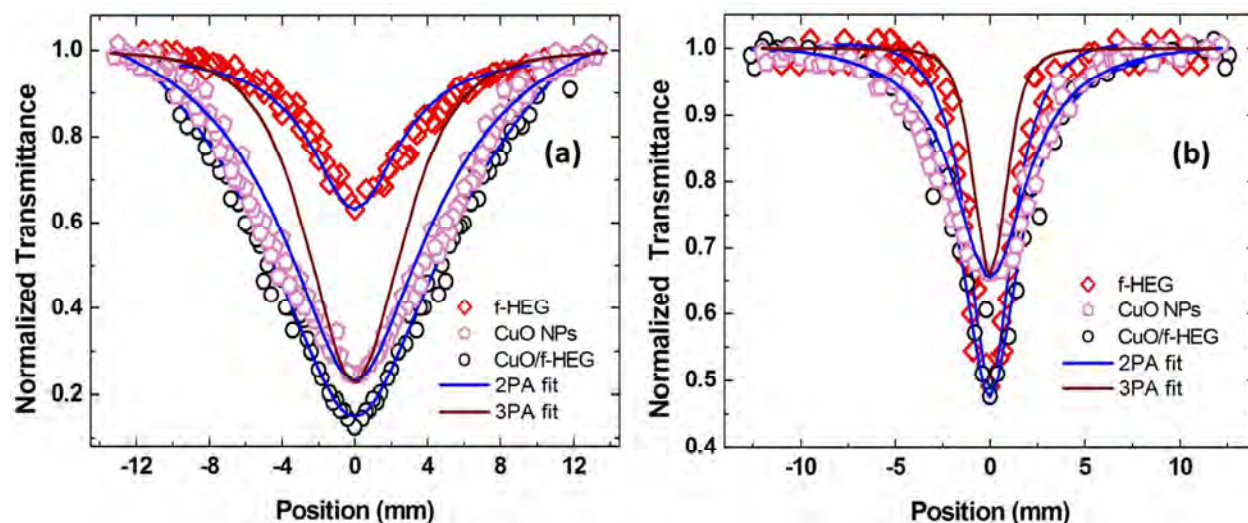


Figure 2. Open aperture Z-scan curves measured for *f*-HEG, CuO NP and CuO/*f*-HEG with (a) 5 ns pulses at 532 nm, and (b) 100 fs pulses at 800 nm. Solid lines are theoretical fits to the Z-scan data. For comparison, the best fit obtained with a three-photon absorption (3PA) equation in the case of CuO NPs is given. It is clear that the 2PA fit is significantly better than the 3PA fit.

In general, a good optical limiter relies on one or more of the NLO processes such as NLA, nonlinear refraction, and induced thermal scattering (ITS) for efficient light attenuation at high intensities. The smooth valley shaped Z-scan curves shown in Figures 2a and 2b which are symmetric about the focal point suggest the relative predominance of NLA. Depending on the material under study, excitation wavelength and pulse width, NLA can happen *via* mechanisms such as multiphoton absorption and/or excited state absorption (ESA). Numerical simulations reveal that the best fit to the present Z-scan data is obtained when a two-photon absorption (2PA) process is considered for both excitation regimes. The transmission of a two-photon absorber is given by¹⁵

$$T = ((1 - R)^2 \exp(-\alpha_0 L) / \sqrt{\pi q_0}) \int_{-\infty}^{+\infty} \ln[1 + q_0^2 \exp(-t^2)] dt \quad (1)$$

where L and R are the sample length and surface reflectivity respectively. α_0 is the linear absorption coefficient and q_0 is given by $\beta(1 - R)I_0 L_{eff}$, where β is the 2PA coefficient. The

effective length L_{eff} is given by $(1 - \exp(-\alpha_o L))/\alpha_o$. The obtained β values are of the order of 10^{-10} m/W in the ns regime and 10^{-14} m/W in the fs regime. However, a good numerical fit of the experimental data to eq. (1) does not necessarily indicate the exclusive occurrence of 2PA; the nonlinearity may have contributions from two-step ESA as well.¹⁶ In fact by making a number of Z-scan measurements at different laser pulse energies and plotting the 2PA coefficients (β) against the corresponding on-axis peak intensities, the true underlying mechanisms of the observed nonlinearity can be elucidated. For instance, the cross section of a genuine two-photon process is too low to deplete the ground state population appreciably, and therefore, for a given excitation wavelength and sample concentration, the variation of β with on-axis peak intensity is negligible. On the other hand, ESA can cause substantial transient depletion of the ground state with pulsed excitation, with the result that β varies with on-axis peak intensity.¹⁷ Our measurements reveal that β indeed varies (decreases) with on-axis peak intensity as shown in Figures 3a and 3b, for fs and ns excitation respectively, indicating the occurrence of ESA in both the excitation regimes. In the case of Pd/f-HEG and Pt/f-HEG hybrids too, NLA coefficients were found to be dependent on on-axis peak intensity wherein β values increase with I_o .⁴ It is important to note that ESA can lead to either an increase or decrease in the β values, as a function of I_o , depending on the absorption cross-sections of the ground state and the excited state, and the excited state lifetimes. Therefore the trend can vary from one material to another.

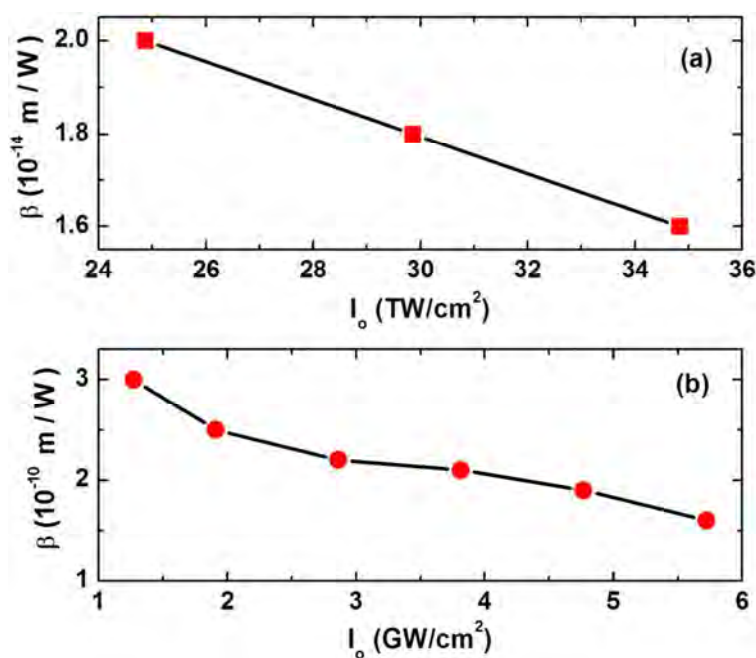


Figure 3. Variation of 2PA coefficient with on-axis peak intensity (I_0) in the (a) fs excitation regime and (b) ns excitation regime, indicating the occurrence of two-step ESA in both cases.

The optical limiting threshold (LT), defined as the input fluence at which the transmittance falls to half the linear transmittance value, can be used for a quantitative comparison of the OL performance of different materials. From the definition it follows that lower the LT value, better the limiting performance. Since LT is dependent on sample linear transmittance, laser pulse width, and excitation wavelength, comparison of the LT values of different optical limiters becomes meaningful only if the measurements are done under similar experimental conditions. In the case of open aperture Z-scan using a Gaussian beam, the input fluence at each z-position is given by $F(z) = 4 \sqrt{\ln 2} E_{in} / \pi^{3/2} w(z)^2$ where E_{in} is the input laser pulse energy and $w(z)$ is the beam radius. A plot of $F(z)$ vs. transmittance yields the optical limiting curve (Figures 4a and 4b), from which the LT values can be found. The values measured in CuO/*f*-HEG for ns and fs excitations are 4.35 J/cm² and 1.43 J/cm² respectively. On the other hand, the LT value obtained in *f*-HEG in the fs excitation regime is 2.7 J/cm², while limiting is not strong enough to estimate LT values in the ns excitation regime. Thus it is clear that CuO decoration has significantly improved the OL performance of *f*-HEG in both excitation regimes. It may be noted that the fs limiting threshold values of CuO/*f*-HEG hybrids are better than those of previously reported benchmark materials like C₆₀ (~2 J/cm²)¹⁸, carbon black (~2.2 J/cm²)¹⁸ and *f*-HEG decorated with metal NPs like Ag (~1.9 J/cm²)⁷, Pt (~1.8 J/cm²)⁴ and Pd (~1.5 J/cm²)⁴, making CuO/*f*-HEG attractive for applications such as eye and sensor protection from hazardous laser radiation. In addition, the β values of CuO/*f*-HEG hybrids in the ns excitation regime are higher than that of other composite systems such as ZnO/reduced graphene oxide⁹ and CdS/graphene¹⁹. Such superior nonlinear behavior is also highly promising for building photonic logic devices such as all-carbon optical diode based on axial asymmetry in nonlinearity.²⁰

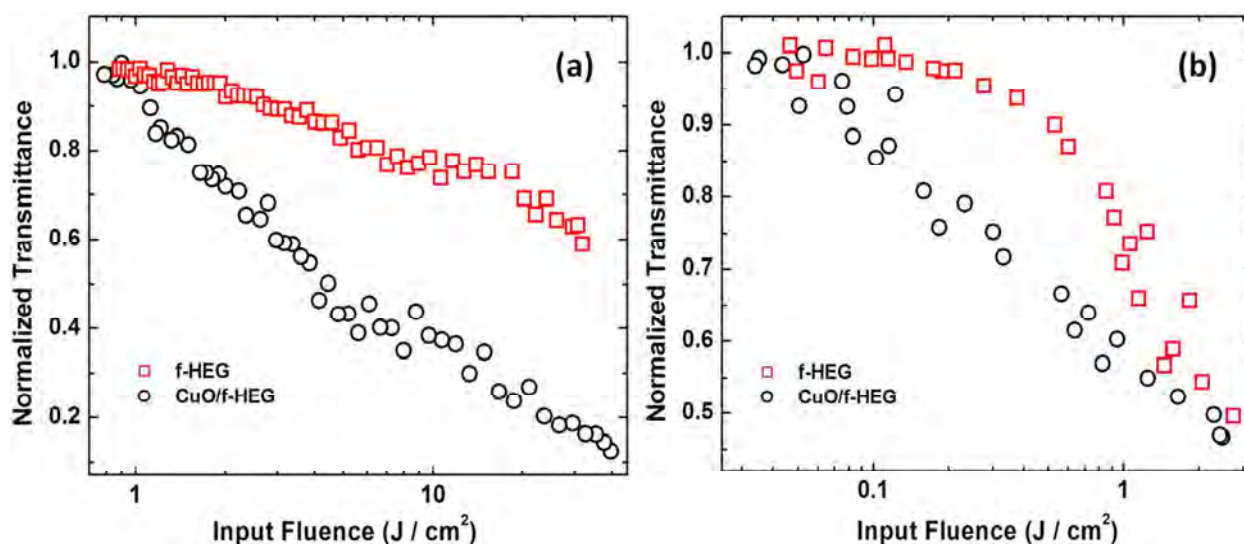


Figure 4. Optical limiting curves of *f*-HEG and CuO/*f*-HEG in the (a) ns excitation regime and (b) fs excitation regime.

Graphene possesses outstanding nonlinear absorption properties by virtue of its unique electronic band structure. Energy dispersion is linear in the vicinity of the *K* point,²¹ which allows for the coupling of any level in the valence band to any desired level in the conduction band by a photon of appropriate energy, enabling wideband tunability. As mentioned before, epitaxial graphene and CVD grown graphene are known to be excellent saturable absorbers. When photoexcited, a non-equilibrium carrier population is produced in the valence band and conduction band of graphene, and once a steady state is reached between excited electrons and electrons relaxing to initial states, further absorption of photons within the pulse width is restricted due to Pauli blocking.²² The increased light transmission thus achieved at higher intensities finds applications in mode-locking,²² pulse shaping and optical switching.²³ On the other hand, HEG shows strong optical limiting due to the large number of defect induced states which enhances NLA, causing attenuation of laser intensity at higher incident fluences.⁴ The mechanism of NLA was found to be ESA in the ns regime, and 2PA combined with saturable absorption (2PA+SA) in the fs regime.⁴ Although HEG contains remnant oxygen functionalities (~6-8 wt. %) even after reduction from GO, they are not sufficient to sustain stable dispersions. But many of the practical applications including optical limiters and nanofluids require long-term stable dispersions.²⁴ Acid functionalization of HEG to form *f*-HEG increases its solubility in solvents, which also helps in the uniformity of metal oxide loading. We have shown previously that increasing defects through acid functionalization is a simple yet excellent method for

improving the OL properties of HEG.⁴ Furthermore, features of the UV-Vis spectrum of *f*-HEG, and increase in the I_D/I_G ratio (0.88 to 1.12), confirm the increase in defect density. The mechanism of NLA in *f*-HEG remains the same as that in HEG.

The observed enhancement in the LT values of MO/*f*-HEG can be primarily attributed to NLA in the CuO NPs. NLA in CuO NPs can be linked to the presence of surface states as discussed below. Photoluminescence studies done by El-Trass *et al.* have revealed the presence of surface states in CuO NPs arising due to oxygen vacancies and Cu interstitials.²⁵ Previously we have shown that NLA in ZnO nanotetrapods is strongly influenced by the surface states induced by Zn interstitials.²⁶ In a similar fashion, the large surface state density could lead to NLA in CuO NPs as well. The reported band gap for CuO NPs of 5-10 nm size is ~ 2.1 eV²⁷, and therefore, ns excitation at 532 nm (2.33 eV) will result in interband transitions between the *d* band and *s-p* conduction band. Subsequent ESA to higher lying states in the conduction band results in NLA as shown in Figure 2. Absorption at 800 nm (1.55 eV) can be attributed to the *d-d* transitions in the partially filled $3d^9$ state of the dispersed Cu^{2+} species.²⁵ Furthermore, in a recent study, Rao and co-workers have shown that when graphene is decorated with metal NPs, charge transfer takes place at the graphene-metal interface to achieve a common Fermi level.²⁸ Charge transfer is from graphene to metal in the case of Ag, Pd and Pt NPs, while for Au NPs it is from metal to graphene. Recently, similar observations are made in the case of metal oxides like ZnO and MoO_3 .^{29,30} Since the work functions of CuO and *f*-HEG are 5.2 eV³¹ and 4.5 eV⁷ respectively, charge transfer from *f*-HEG to CuO NPs is likely in the present case. The transferred excited carriers from *f*-HEG undergo subsequent ESA transitions in the large density of metal oxide states, leading to an overall increase in NLA in the composite system, which in turn results in an improved OL performance.

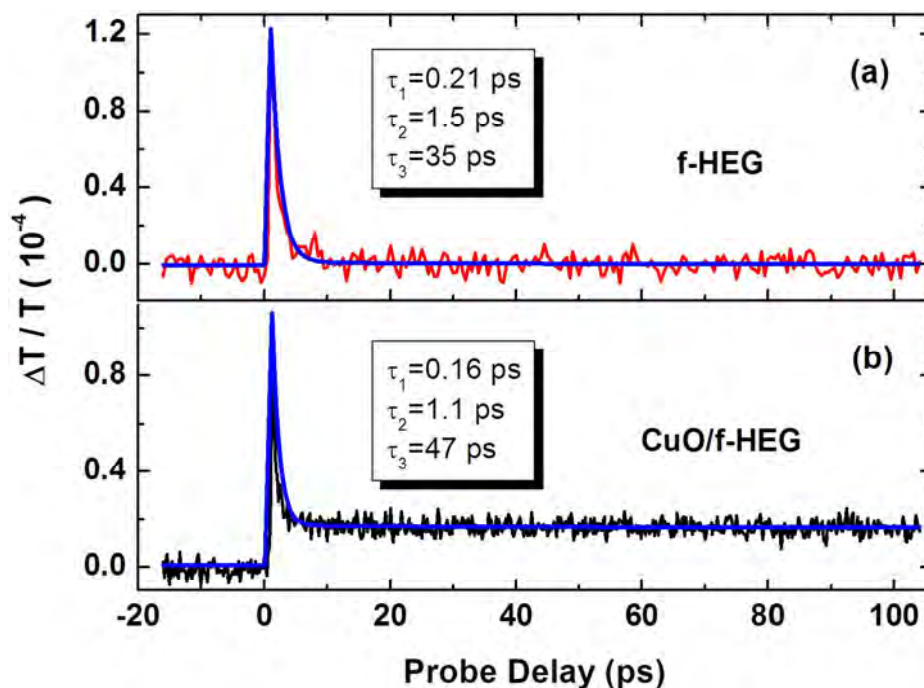


Figure 5. Ultrafast time-resolved differential transmission data of *f*-HEG and CuO/*f*-HEG measured at 580 nm. Solid lines are tri-exponential fits to the experimental data. The effect of metal oxide decoration is clearly reflected in the carrier relaxation lifetimes.

3.3. Carrier dynamics in *f*-HEG and CuO/*f*-HEG

The ultrafast transient differential transmission spectra ($\Delta T(t)/T$) of *f*-HEG and CuO/*f*-HEG measured from degenerate pump-probe measurements are given in Figure 5. Here T is the probe transmission in the absence of pump beam and $\Delta T(t)$ is the change in probe transmission at time t after excitation by the pump. The differential transmission data is fitted with a tri-exponentially decaying function $\Delta T/T = A_1 \exp(-t/\tau_1) + A_2 \exp(-t/\tau_2) + A_3 \exp(-t/\tau_3)$ as shown in Figure 5. The three distinct decay time constants obtained from the best fits provide information regarding various relaxation mechanisms. In the case of *f*-HEG (see Figure 5a), the fast component τ_1 (210 fs) can be attributed to interband carrier-carrier scattering, while the slow component τ_2 (1.5 ps) arises from carrier-phonon scattering.^{32,33} The third component τ_3 of the time decaying function is much slower (35 ps), and it can be associated with carrier trapping by defect states, which arises from oxygen functionalities and other structural defects.³² Such trap states are found to play a major role in prolonging carrier relaxation in reduced graphene oxide to

the range of 30-400 ps.³⁴ As mentioned before, the strong OL in HEG and *f*-HEG arises mainly due to the ESA mediated by these defect induced states.⁴

In general, carrier dynamics in graphene and reduced graphene oxide can be described as follows. Intraband and interband one-photon and two-photon absorption processes during photo-excitation lead to a narrow non-equilibrium carrier distribution in the valence and conduction bands of graphene.³⁵ The carriers quickly equilibrate in a timescale of 10-200 fs *via* inelastic and elastic intraband carrier-carrier scattering to reach a hot Fermi-Dirac distribution.³⁵ Subsequently, these hot electrons cool down in a timescale of 1-2 ps by interband carrier-phonon scattering involving both optical and acoustic phonons, reaching thermal equilibrium with the lattice.²⁷ In the case of carrier trapping by trap states, carrier relaxation to the ground state gets delayed by hundreds of ps, up to a few ns.^{34,36} An important factor determining carrier dynamics in graphene is the defect density. Ultrafast time resolved measurements carried out in epitaxial graphene by Dawlaty *et al.* reveal that carrier relaxation times decrease with increase in defects (i.e, increase in the I_D/I_G ratio) in the graphene lattice that reduces the in-plane crystallite size.³² As mentioned before, I_D/I_G ratio of *f*-HEG reduces from 1.12 ± 0.03 to 0.95 ± 0.02 upon metal oxide loading because the CuO NPs attach to the dangling bonds at the edges of *f*-HEG sheets.¹⁴ Therefore the reduction in τ_1 and τ_2 values observed with CuO/*f*-HEG is not due to the effect of defects, but due to higher carrier density in CuO/*f*-HEG compared to *f*-HEG.³² The increase in τ_3 can be associated with the longer lived trap states in CuO nanoparticles which further delay carrier relaxation.³⁷

3.4. Contribution of induced thermal scattering towards optical limiting

Many of the previously reported NLO studies on graphene based nanocarbon suspensions revealed that induced thermal scattering (ITS) is the predominant mechanism contributing to observed OL.^{38,39} When excited with intense laser pulses, graphene flakes get heated up and transfer the heat energy to the surrounding solvent. This localized heating leads to the formation of solvent bubbles which expand quickly due to the large pressure difference at the vapor-solution interface. When the size of the solvent bubbles becomes comparable to the excitation wavelength, they reduce the light transmission considerably due to Mie scattering. Alternatively, the intense photon flux can ionize the graphene flakes directly, forming rapidly expanding micro-plasma which also acts as scattering centers.^{39, 40} In general, scattering centers take several

nanoseconds for their formation. Therefore the effect of ITS is significant only in ns or longer pulse excitation regimes.

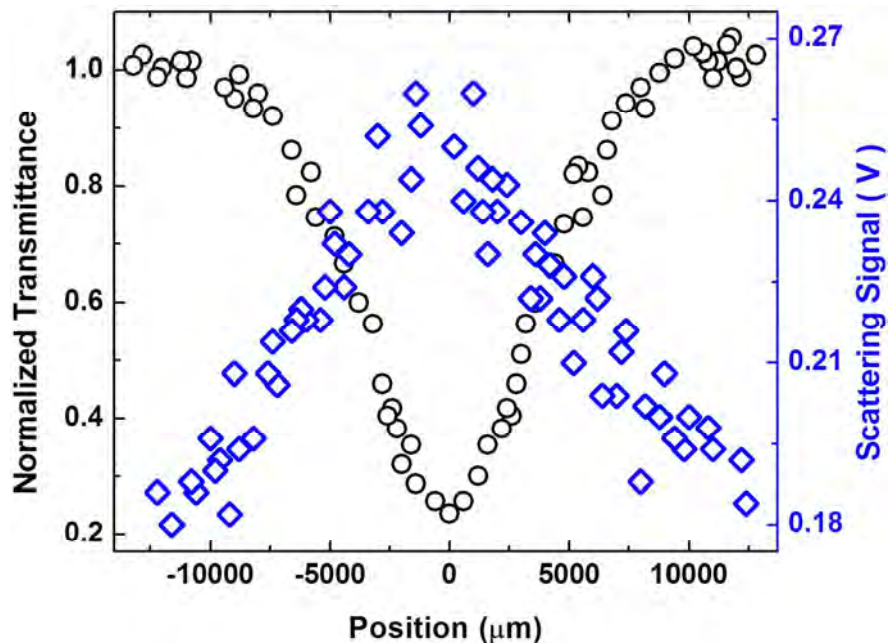


Figure 6. Open aperture Z-scan (circles) and induced thermal scattering (squares) measured in CuO/*f*-HEG excited by ns laser pulses with an on-axis peak intensity of 4.77 GW/cm^2 . The ITS signal variation is not large enough to cause the observed limiting strength, indicating that the nonlinearity arises mostly from NLA.

In order to study the contribution of ITS towards the OL performance of CuO/*f*-HEG, we measured the variation of light scattering from the dispersion during a ns Z-scan run with an on-axis peak intensity of 4.77 GW/cm^2 . A photodiode kept close to the sample at an angle of 45° to the beam axis was used for the measurements. The measured scattering signal is plotted in Figure 6. The variation in signal amplitude, which is from 0.18 to 0.26 V, is not significant enough to contribute substantially to the observed optical limiting. This suggests a weak ITS compared to NLA in the present case. This is also indirectly evident from the fact that the 2PA equation fits to the Z-scan data very well. In fact the laser beam transmitted through the sample maintains the same transverse profile visibly, indicating negligible distortions due to scattering. Previous studies done on *f*-HEG and metal/*f*-HEG hybrids also showed negligible contribution of ITS towards OL.^{4,7} This is mainly due to the fact that, compared to the earlier studies done on graphene suspensions containing isolated particles, here we have used stable dispersions of high

thermal conductivity which act as thermally homogenous media with better thermal diffusion. In fact, thermal conductivity and heat transfer coefficient of CuO/*f*-HEG are higher than those of *f*-HEG.³ As a result heat generated locally by ns excitation will be dissipated evenly to the surroundings easily, thereby reducing the formation of localized scattering centers. Moreover the measurements were carried out in the single-shot mode so that only one laser pulse is incident on the sample in every 2 seconds: in this way chances of accumulative thermal effects are minimized. Therefore the observed OL in CuO/*f*-HEG primarily occurs from strong NLA in both the ultrafast and short-pulse excitation regimes.

4. CONCLUSIONS

In conclusion, nonlinear optical properties of CuO/*f*-HEG hybrids have been studied using the open aperture Z-scan technique in both ultrafast (fs) and short-pulse (ns) laser excitation regimes. The excellent optical limiting response measured in CuO/*f*-HEG is attributed to (a) strong nonlinear absorption in HEG mediated by defect induced states which increase in number by acid functionalization, (b) nonlinear absorption in CuO nanoparticless due to excited state absorption, and (c) charge transfer between *f*-HEG and CuO nanoparticles. Ultrafast carrier dynamics measurements confirm the role of defect induced states which prolong the relaxation dynamics by carrier trapping. Contribution of induced thermal scattering towards the observed optical limiting is negligible due to the fine dispersibility of the samples in water, combined with their very good thermal transport properties. The present study reveals that metal oxide decoration is an effective method for making excellent optical limiters using hydrogen exfoliated graphene.

■ AUTHOR INFORMATION

Corresponding Author

*E-mail: reji@rri.res.in

■ ACKNOWLEDGEMENTS

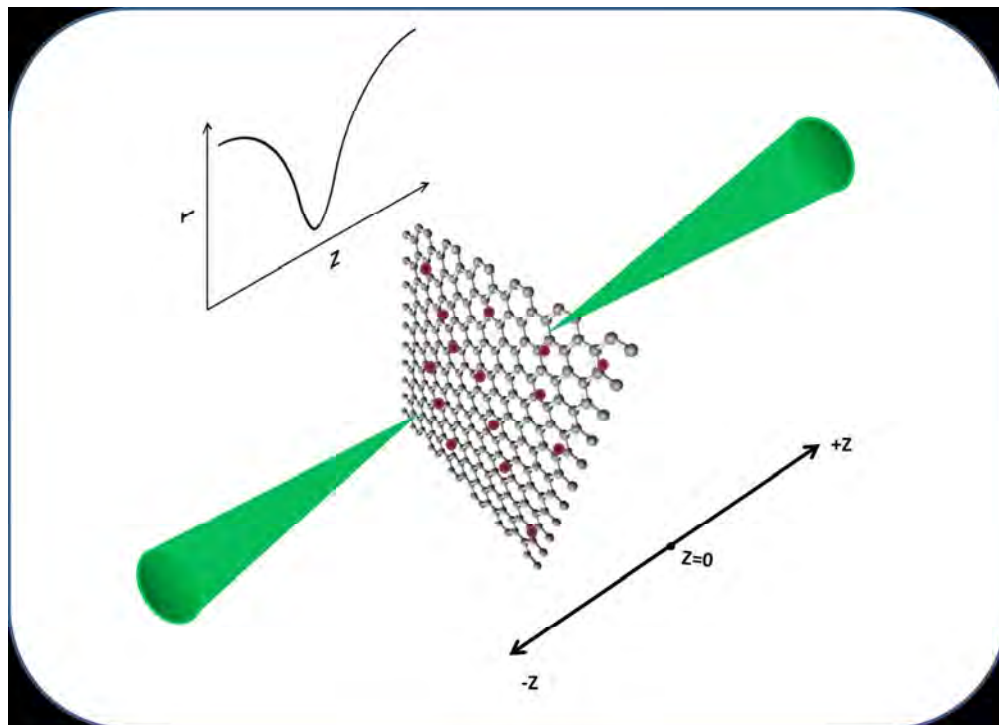
B.A. and S.S.S.S. are grateful to Sri Sathya Sai Baba, the founder chancellor of SSSIHL, for support and lab facilities. B.A. acknowledges UGC, India for a senior research fellowship. Authors from IITM thank IITM, DST, and Defense Research Development Organization (DRDO), India for financial and infrastructural support.

REFERENCES

1. A. Kaniyoor, T. T. Baby, T. Arockiadoss, N. Rajalakshmi and S. Ramaprabhu, *J. Phys. Chem. C*, 2011, **115**, 17660.
2. T. T. Baby and S. Ramaprabhu, *Appl. Phys. Lett.*, 2011, **98**, 183111.
3. T. T. Baby and S. Ramaprabhu, *J. Phys. Chem. C*, 2011, **115**, 8527.
4. B. Anand, A. Kaniyoor, S. S. S. Sai, R. Philip and S. Ramaprabhu. *J. Mat. Chem. C* 2013, **1**, 2773.
5. G. Xing, H. Guo, X. Zhang, T. C. Sum and C. H. A. Huan, *Opt. Express*, 2010, **18**, 4564.
6. R. Podila, B. Anand, J. T. Spear, P. Puneet, R. Philip, S. S. S. Sai and A. M. Rao, *Nanoscale*, 2012, **4**, 1770.
7. B. S. Kalanoor, P. B. Bisht, S. A. Ali, T. T. Baby and S. Ramaprabhu, *J. Opt. Soc. Am. B*, 2012, **29**, 669.
8. M. Ando, K. Kadono, M. Haruta, T. Sakaguchi and M. Miya, *Nature*, 1995, **374**, 625.
9. M. K. Kavitha, H. John, P. Gopinath and R. Philip, *J. Mater. Chem. C*, 2013, **1**, 3669.
10. C. -T. Hsieh, J. -M. Chen, H. -H. Lin and H. -C. Shih, *Appl. Phys. Lett.*, 2003, **83**, 3383.
11. J. Morales, L. Sánchez, F. Martín, J. R. Ramos-Barrado and M. Sánchez, *Thin Solid Films*, 2005, **474**, 133.
12. V. S. Muthukumar, R. Podila, B. Anand, B, S. S. S. Sai, K. Venkataramaniah, R. Philip and A. M. Rao, *Encyclopedia of Nanotechnology*; Springer-Verlag: Heidelberg, 2013.

13. D. Swain, P. T. Anusha, T. S. Prashant, S. P. Tewari, T. Sarma, P. K. Panda and S. Venugopal Rao, *Appl. Phys. Lett.*, 2012, **100**, 141109.
14. Y. M. Ho, J. W. Liu, J. L. Qi and W. T. Zheng, *J. Phys. D: Appl. Phys.*, 2008, **41**, 065308.
15. R. L. Sutherland, *Handbook of Nonlinear Optics*; Marcel Dekker Inc.: New York, 1996.
16. M. Rumi and J. W. Perry, *Adv. Opt. Photon.*, 2010, **2**, 451.
17. B. Anand, R. Podila, P. Ayala, L. Oliveira, R. Philip, S. S. S. Sai and A. M. Rao, *Nanoscale*, 2013, **5**, 7271.
18. P. Chen, X. Wu, X. Sun, J. Lin, W. Ji and K. L. Tan, *Phys. Rev. Lett.*, 1999, **82**, 2548.
19. F. Miao, S. Ruiqing, Z. Hongbing and C. Yu, *Nanotechnology*, 2010, **21**, 075601.
20. B. Anand, R. Podila, K. Lingam, S. R. Krishnan, S. S. S. Sai, R. Philip and A. M. Rao, *Nano Lett.* 2013, **13**, 5771.
21. A. H. C. Neto, F. Guinea, N. M. R. Peres, K. S. Novoselov and A. K. Geim, *Rev. Mod. Phys.*, 2009, **81**, 109.
22. Q. Bao, H. Zhang, Y. Wang, Z. Ni, Y. Yan, Z. X. Shen, K. P. Loh and D. Y. Tang, *Adv. Funct. Mater.*, 2009, **19**, 3077.
23. Q. Bao and K. P. Loh, *ACS Nano*, 2012, **6**, 3677.
24. M. -C. Hsiao, S. -H. Liao, M. -Y. Yen, P. -I. Liu, N. -W. Pu, C. -A. Wang and C. -C. M. Ma, *ACS Appl. Mater. Interfaces*, 2010, **2**, 3092.
25. A. El-Trass, H. ElShamy, I. El-Mehasseb and M. El-Kemary, *Appl. Surf. Sci.*, 2012, **258**, 2997.
26. M. Egblewogbe, B. Anand, R. Podila, R. Philip, S. S. S. Sai and A. M. Rao, *Mater. Express*, 2012, **2**, 351.
27. A. Chen, G. Yang, H. Long, F. Li, Y. Li and P. Lu, *Thin Solid Films*, 2009, **517**, 4277.
28. K. S. Subrahmanyam, A. K. Manna, S. K. Pati and C. N. R. Rao, *Chem. Phys. Lett.*, 2010, 497, 70.

29. H. Hayashi, I. V. Lightcap, M. Tsujimoto, M. Takano, T. Umeyama, P. V. Kamat and H. Imahor, *J. Am. Chem. Soc.*, 2011, **133**, 7684.
30. J. Meyer, P. R. Kidambi, B. C. Bayer, C. Weijtens, A. Kuhn, A. Centeno, A. Pesquera, A. Zurutuza, J. Robertson and S. Hofmann, *Sci. Rep.*, 2014, **4**, 5380.
31. L. Liao, Z. Zhang, B. Yan, Z. Zheng, Q.L. Bao, T. Wu, C.M. Li, Z.X. Shen, J.X. Zhang, H. Gong, J.C. Li and T. Yu, *Nanotechnology*, 2009, **20**, 085203.
32. J. M. Dawlaty, S. Shivaraman, Mvs. Chandrashekhar, F. Rana and M. G. Spencer, *Appl. Phys. Lett.*, 2008, **92**, 042116.
33. S. Kumar, M. Anija, N. Kamaraju, K. S. Vasu, K. S. Subrahmanyam, A. K. Sood and C. N. R. Rao, *Appl. Phys. Lett.*, 2009, **95**, 191911.
34. S. Kaniyankandy, S. N. Achary, S. Rawalekar and H. N. Ghosh, *J. Phys. Chem. C*, 2011, **115**, 19110.
35. H. Yang, X. Feng, Q. Wang, H. Huang, W. Chen, A. T. S. Wee and W. Ji, *Nano Lett.*, 2011, **11**, 2622.
36. G. -K. Lim, Z. -L. Chen, J. Clark, R. G. S. Goh, W. -H. Ng, H. -W. Tan, R. H. Friend, P. K. H. Ho and L. -L. Chua, *Nat. Photon.*, 2011, **5**, 554.
37. Y. Lou, M. Yin, S. O'Brien and C. Burda, *J. Electrochem. Soc.*, 2005, **152**, G427.
38. M. Feng, H. Zhan and Y. Chen, *Appl. Phys. Lett.*, 2010, **96**, 033107.
39. J. Wang, Y. Hernandez, M. Lotya, J. N. Coleman and W. J. Blau, *Adv. Mater.*, 2009, **21**, 2430.
40. K. Mansour, M. J. Soileau and E. W. Van Stryland, *J. Opt. Soc. America B-Opt. Phys.* 1992, **9**, 1100.



Enhancing the nonlinear absorption in hydrogen exfoliated graphene using metal oxide nanoparticle functionalization
229x165mm (150 x 150 DPI)